AGU PUBLICATIONS

JGR

Journal of Geophysical Research: Atmospheres

RESEARCH ARTICLE
10.1002/2013JD021403

Key Points:
- Stratospheric easterly change is common feature in future climate projections
- Significant intermodel spread in stratospheric northern winter climate change
- Importance of stratospheric easterly change to narrow uncertainty in SLP change

Correspondence to:
E. Manzini,
elisa.manzini@mpimet.mpg.de

Citation:
Manzini, E., et al. (2014), Northern winter climate change: Assessment of uncertainty in CMIP5 projections related to stratosphere-troposphere coupling, *J. Geophys. Res. Atmos.*, *119*, doi:10.1002/2013JD021403.

Received 20 DEC 2013
Accepted 10 JUN 2014
Accepted article online 12 JUN 2014

Northern winter climate change: Assessment of uncertainty in CMIP5 projections related to stratosphere-troposphere coupling

E. Manzini[1], A. Yu. Karpechko[2], J. Anstey[3], M. P. Baldwin[4], R. X. Black[5], C. Cagnazzo[6], N. Calvo[7], A. Charlton-Perez[8], B. Christiansen[9], Paolo Davini[10], E. Gerber[11], M. Giorgetta[1], L. Gray[3], S. C. Hardiman[12], Y.-Y. Lee[13], D. R. Marsh[14], B. A. McDaniel[15], A. Purich[16], A. A. Scaife[12], D. Shindell[17], S.-W. Son[18], S. Watanabe[19], and G. Zappa[20]

[1]Max Planck Institute for Meteorology, Hamburg, Germany, [2]Finnish Meteorological Institute, Helsinki, Finland, [3]Department of Physics, University of Oxford, Oxford, UK, [4]College of Engineering, Mathematics and Physical Sciences, University of Exeter, Exeter, UK, [5]School of Earth and Atmospheric Sciences, Georgia Institute of Technology, Atlanta, Georgia, USA, [6]Istituto di Scienze dell'Atmosfera e del Clima, Consiglio Nazionale delle Ricerche, Rome, Italy, [7]Departamento de Fisica de la Tierra II, Universidad Complutense de Madrid, Madrid, Spain, [8]Department of Meteorology, University of Reading, Reading, UK, [9]Danish Meteorological Institute, Copenhagen, Denmark, [10]Istituto di Scienze dell'Atmosfera e del Clima, Consiglio Nazionale delle Ricerche, Torino, Italy, [11]Courant Institute of Mathematical Sciences, New York University, New York, New York, USA, [12]Met Office Hadley Centre, Exeter, UK, [13]Department of Land, Air and Water Resources, University of California, Davis, California, USA, [14]National Center for Atmospheric Research, Boulder, Colorado, USA, [15]Department of Biology and Physics, Kennesaw State University, Kennesaw, Georgia, USA, [16]CSIRO Marine and Atmospheric Research, Aspendale, Victoria, Australia, [17]Goddard Institute for Space Studies, NASA, New York, New York, USA, [18]School of Earth and Environmental Sciences, Seoul National University, Seoul, South Korea, [19]Japan Agency for Marine-Earth Science and Technology, Yokohama, Japan, [20]National Centre for Atmospheric Science, University of Reading, Reading, UK

Abstract Future changes in the stratospheric circulation could have an important impact on northern winter tropospheric climate change, given that sea level pressure (SLP) responds not only to tropospheric circulation variations but also to vertically coherent variations in troposphere-stratosphere circulation. Here we assess northern winter stratospheric change and its potential to influence surface climate change in the Coupled Model Intercomparison Project-Phase 5 (CMIP5) multimodel ensemble. In the stratosphere at high latitudes, an easterly change in zonally averaged zonal wind is found for the majority of the CMIP5 models, under the Representative Concentration Pathway 8.5 scenario. Comparable results are also found in the 1% CO_2 increase per year projections, indicating that the stratospheric easterly change is common feature in future climate projections. This stratospheric wind change, however, shows a significant spread among the models. By using linear regression, we quantify the impact of tropical upper troposphere warming, polar amplification, and the stratospheric wind change on SLP. We find that the intermodel spread in stratospheric wind change contributes substantially to the intermodel spread in Arctic SLP change. The role of the stratosphere in determining part of the spread in SLP change is supported by the fact that the SLP change lags the stratospheric zonally averaged wind change. Taken together, these findings provide further support for the importance of simulating the coupling between the stratosphere and the troposphere, to narrow the uncertainty in the future projection of tropospheric circulation changes.

1. Introduction

The potential importance of future stratospheric mean changes driven by increased greenhouse gases for surface climate change in the northern extratropics has been illustrated by many studies including the recent one by *Scaife et al.* [2012]. While previous works addressed the role of stratospheric change with individual models, Scaife et al. included a multimodel intercomparison of Coupled Model Intercomparison Project-Phase 3 (CMIP3) and Chemistry Climate Model Validation (CCMVal) simulations. From their intercomparisons, they deduced that changes in the stratospheric circulation have the effect of substantially reducing projected changes in sea level pressure (SLP) both in the Arctic and at midlatitudes in winter, with potentially large impacts on the projected frequency of extreme winter weather events in the North Atlantic-European region. The CCMVal models [*SPARC CCMVal*, 2010] extend higher in the atmosphere to include the full extent of the stratosphere, in contrast to the CMIP3 models [*Cordero and de Forster*, 2006]. The *Scaife et al.* [2012] results,

©2014. American Geophysical Union. All Rights Reserved.

augmented by their comparison between two pairs of high/low top atmospheric models, therefore imply that it is important to resolve the stratosphere in climate models used for predicting the circulation response to climate change at the regional scale.

The stratospheric changes driving the surface impacts found in the Northern Hemisphere, by *Scaife et al.* [2012] and others, are linked to weakening (easterly change) of the high-latitude stratospheric winds in a future climate. It seems, therefore, that stratosphere-troposphere coupling for the mean changes projects on the well-known coupling patterns of intraseasonal variability [*Baldwin and Dunkerton*, 2001]. Also, *Karpechko and Manzini* [2012, hereafter KM12] found that the weakening of stratospheric winds in response to increased CO_2 concentration primarily occurs in early winter (November–December). The early winter stratospheric changes then slowly progress downward and the influence of the stratospheric response maximizes in midwinter and later winter (January to March) at the surface. There is indeed compelling evidence that the Baldwin Dunkerton relationship (i.e., stratosphere-troposphere dynamical coupling at intraseasonal time scale, including the lag in the response) holds on longer timescales from analysis of the Southern Hemisphere, where ozone loss-induced cooling causes a poleward shift in the tropospheric subtropical jet [*Thompson and Solomon*, 2002; *Son et al.*, 2010].

However, the robustness of the easterly change for zonal mean zonal winds has not been fully established. Although most of recent analyses point to an easterly change (KM12 for a brief review), the stratospheric influence deduced by the early work of *Shindell et al.* [1999] would be linked to a strengthening of high-latitude stratospheric winds in a future climate. So far, there is limited consensus on likely future changes in sudden stratospheric warming frequency (KM12 and references therein). Direct or indirect (e.g., via their influence on the mean flow) impacts from gravity wave parameterizations are likely to be an important factor and add uncertainty [*Shaw et al.*, 2009; *Sigmond and Scinocca*, 2010].

The first aim of this work is therefore to understand if such an easterly change during northern winter is robustly predicted by the majority of climate models in the latest set of climate projections, carried out under the fifth Coupled Model Intercomparison Project (CMIP5). The motivation to assess the CMIP5 multimodel ensemble is because, in contrast to previous CMIP multimodel ensembles, CMIP5 includes a large fraction of models that extend above the stratopause [*Gerber et al.*, 2012; *Charlton-Perez et al.*, 2013]. We find indeed that the CMIP5 multimodel mean predicts a weakening of the high-latitude zonally averaged stratospheric zonal winds not previously present in the CMIP3 models (sections 3 and 4). However, there is a substantial intermodel spread in the response of the high-latitude stratospheric winds, even in the sign of the response.

The second aim of this work is then to explore if the intermodel spread in the projected stratospheric mean changes can contribute to the spread in tropospheric circulation changes and can be attributed to differences in model formulations. The motivation of this aim is to search for evidence, within the CMIP5 multimodel ensemble, of the potential to narrow the uncertainty in the future projection of seal level pressure (SLP) changes by reducing the spread in stratospheric mean change. In case such evidence is found, our results will strongly motivate further investigation of the origin of the stratospheric zonally averaged changes and of the definition of the model requirements to capture them. These questions are beyond the goals of this work and left for future research. We currently limit us to note that the stratosphere-troposphere coupling involved in the stratospheric mean changes can be two-way and can involve a time lag between the upward and downward couplings [*Reichler et al.*, 2005]. Tropospheric precursors, as in the case of intraseasonal variability [*Polvani and Waugh*, 2004], can therefore be involved. Moreover, the modeling of the whole interaction cycle (troposphere to stratosphere to troposphere) may depend, among other factors, on the climatological atmospheric mean state [*Sigmond and Scinocca*, 2010] and is not necessarily well captured in models only partially resolving stratospheric processes [*Scaife et al.*, 2012; KM12; *Cagnazzo and Manzini*, 2009; *Omrani et al.*, 2014].

The main atmospheric changes that can impact the tropospheric extratropical circulation response to anthropogenic climate change are (1) tropical upper troposphere warming, which causes the well-known pattern of lower/higher SLP over the pole/midlatitudes in a future climate [*Meehl et al.*, 2007; *Butler et al.*, 2010; *Arblaster et al.*, 2011] and (2) polar amplification, whose effects on SLP are less established [*Woollings*, 2008; *Kumar et al.*, 2010; *Screen et al.*, 2013]. In order to isolate the possible consequences of the intermodel spread in projected stratospheric mean changes on SLP, we therefore apply a sequential regression across the model responses. The sequential regression (section 2) is designed to remove the signature of both the tropical upper troposphere warming and polar amplification prior to the analysis of signals of stratosphere-troposphere coupling.

©2014. American Geophysical Union. All Rights Reserved.

Table 1. Models Used in the CMIP3 and CMIP5 Comparison (1% CO_2 Increase per Year Projections)

Institution	CMIP3 MODEL	CMIP5 MODEL
BCC CMA		bcc-csm1-1
CCCMA	cgcm3_1	CanESM2
CNRM-CERFACS	cnrm_cm3	CNRM-CM5
NOAA GFDL	gfdl_cm2_0	
	gfdl_cm2_1	
NASA GISS	giss_model_e_r	
INGV	ingv_echam4	
MOHC	ukmo_hadgem1	HadGEM2-ES
INM	inmcm3_0	inmcm4
IPSL	ipsl_cm4	IPSL-CM5A-LR
		IPSL-CM5A-MR
MIROC	miroc3_2_medres	MIROC5
		MIROC-ESM
FUB	miub_echo_g	
MPI-M	mpi_echam5	MPI-ESM-LR
		MPI-ESM-P
MRI	mri_cgcm2_3_2a	MRI-CGCM3
NCAR	ncar_ccsm3_0	
	ncar_pcm1	
NCC		NorESM1-M
		NorESM1-ME

An alternative approach could be to subdivide the CMIP5 ensemble in two subsets, following the location of the model top [*Charlton-Perez et al.*, 2013]. However, intermodel differences in climate sensitivity, and therefore in global surface warming, can dominate the response of subsets and so lead to erroneous interpretation [*McLandress et al.*, 2012; *Previdi and Polvani*, 2012]. That this is the case for the CMIP5 high and low top model subsets is shown in section 5. Given that there is no theoretical evidence to implicate stratospheric processes in intermodel differences in climate sensitivity, the high/low top subdivision cannot be applied in our investigation. In addition, *Charlton-Perez et al.* [2013] found that while stratospheric variability at all time scales is better simulated in the CMIP5 models with tops above the stratopause (the high top models), the stratospheric mean flow climatology is improved in all CMIP5 models with respect to CMIP3. Given that the stratospheric mean state can be important for the prediction of the stratospheric change [*Sigmond and Scinocca*, 2010], the high/low top subdivision can therefore not sufficiently discriminate the performance of the CMIP5 models in the stratosphere.

2. Methods

The central part of our analysis, the sequential regression and the time-lagged correlation (section 4), focuses on future climate projections and uses the historical simulations from 1961 to 2005, and thereafter the Representative Concentration Pathways 8.5 scenario (RCP8.5), in which year 2100 has a nominal radiative forcing of 8.5 W m^{-2} [*Taylor et al.*, 2012].

Table 2. CMIP5 Models Used in Projections RCP8.5 and Historical Simulations

Institution	Model	Top	Levels
BCC CMA	bcc-csm1-1	2.917 hPa	26
CCCMA	CanESM2	1 hPa	35
NCAR	CCSM4	2.194 hPa	27
CMCC	CMCC-CESM	0.01 hPa	39
	CMCC-CESM-LOW	10 hPa	19
	CMCC-CMS	0.01 hPa	95
CNRM-CERFACS	CNRM-CM5	10 hPa	31
CSIRO-QCCCE	CSIRO-Mk3-6-0	4.52 hPa	18
EC-Earth consortium	EC-EARTH-HIGH	0.01 hPa	91
	EC-EARTH-LOW	5 hPa	62
NASA GISS	GISS-E2-R	0.1 hPa	40
MOHC	HadGEM2-CC	85 km	60
	HadGEM2-ES	40 km	38
INM	inmcm4	10 hPa	21
IPSL	IPSL-CM5A-LR	0.04 hPa	39
	IPSL-CM5A-MR	0.04 hPa	39
MIROC	MIROC5	3 hPa	56
	MIROC-ESM-CHEM	0.0036 hPa	80
	MIROC-ESM	0.0036 hPa	80
MPI-M	MPI-ESM-LR	0.01 hPa	47
	MPI-ESM-MR	0.01 hPa	95
MRI	MRI-CGCM3	0.01 hPa	48
NCC	NorESM1-M	3.54 hPa	26
NCAR	WACCM4	5.1×10^{-6} hPa	66

To put the results of the CMIP5 future climate projections into context with previous CMIP projections, we start in section 3 by comparing mean changes from the idealized simulations in which the CO_2 concentration is increased by 1% per year, common to both CMIP5 and CMIP3. The 1% CO_2 increase per year experiments are initialized from preindustrial control simulations and then run for 140 years, reaching $4 \times CO_2$ levels by the end of the simulations [*Taylor et al.*, 2012]. The change due to the CO_2 increase is computed as the difference between the average of years 101–140 and years 1–40, and only the December to February average is considered. Averages over 40 year periods are used to remove interannual

©2014. American Geophysical Union. All Rights Reserved.

variability. For this analysis, outputs for 15 CMIP3 models and 14 CMIP5 models were available, one realization per model (Table 1).

In the analysis of future climate projections, the change in the atmospheric circulation due to the RCP8.5 forcing is defined as the difference between averages of the RCP8.5 run between 2061 and 2100 and the historical runs between 1961 and 2000. The models used are listed in Table 2. If multiple realizations from the same model are available (CanESM2: 5 runs; CCSM4: 5; CNRM-CM5: 3; HadGEM2-CC: 3; HadGEM2-ES: 3; IPSL-CM5A-LR: 4; and MPI-ESM-LR: 2), their average is used. The residual vertical velocity (diagnostic used in Figures 8 and 9) is a derived variable, not available from the CMIP5 archive, and has been kindly provided by modeling centers. This has been possible only for a limited number of models (one realization per model): CMCC-CESM, CMCC-CMS, EC-EARTH-LOW, GFDL-CM3, GISS-E2-R, HadGEM2-CC, HadGEM2-ES, inmcm4, MIROC-ESM-CHEM, MIROC-ESM, MPI-ESM-LR, MRI-CGCM3, and WACCM4).

2.1. Sequential Regression of December to February Averaged Fields

Zonally averaged temperature and zonal wind changes, and maps (20°N–90°N) of the SLP changes are sequentially regressed on localized mean changes in the atmospheric circulation across all the available models. The changes considered, described below, are defined to characterize upper troposphere warming, polar amplification, and high-latitude stratospheric wind change. Each change is calculated across all the available models and then standardized with respect to its multimodel mean (normalized anomalies to their respective multimodel means).

Δ*T300 change:* following *Arblaster et al.* [2011], who reported that the response of the Southern Annular Mode to global warming across CMIP3 models is related to the simulated upper tropospheric warming in the tropics, we assume that a similar relation exists between the tropical warming and extratropical circulation changes in the Northern Hemisphere (see also *Butler et al.* [2010] for supporting evidence by means of idealized calculation of the circulation response to upper troposphere warming). Therefore, we introduce the ΔT300 change, defined as the DJF change in zonal mean temperature at 300 hPa and averaged between 30°S and 30°N.

Δ*AMPL change:* we introduce the ΔAMPL change to describe the effects of Arctic amplification of near-surface air temperature change on circulation changes. ΔAMPL is defined as the change in temperature at 850 hPa, averaged between 60°N and 90°N. Near-surface Arctic amplification is primarily driven by sea ice loss [*Kumar et al*., 2010; *Screen and Simmonds*, 2010], although other factors, such as the water vapor feedback, may contribute. We use a temperature-based change, as we are interested in the circulation changes induced by the near-surface temperature warming and not in the causes of the warming itself.

Δ*SUA change:* the stratospheric zonal wind change, ΔSUA, is defined as the change in zonal mean zonal wind at 10 hPa, averaged over 70°N–80°N. ΔSUA is designed to identify relationships linked to high-latitude stratospheric wind changes. Prior to the regression, the sign of the ΔSUA change is reversed, so that positive ΔSUA indicates that the projected high-latitude zonal winds weaken in the future (and easterly change). The 10 hPa level is used for practical reasons, because it is the uppermost level reported from all models. The stratospheric high-latitude changes are coherent throughout the stratosphere, as attested by the models for which outputs at pressures less than 10 hPa are available (not shown), which suggests that the results should be insensitive to the level chosen in defining the ΔSUA change. The 70°–80°N latitudinal band is chosen to focus on polar changes (but tests confirmed that the results are not sensitive to the precise latitude range employed).

In summary, the signals of intermodel spread associated with the tropical upper troposphere warming and Arctic amplification are removed by regressing the variables of interest on the ΔT300 and subsequently the ΔAMPL changes on the ΔT300 residuals (Figures 3a–3d, 4a–4d, and 5a–5d). The residual fields after this second regression are thereafter used to search for signals of stratosphere-troposphere coupling (Figures 3e, 3f, 4e, 4f, 5e, and 5f). The success of the sequential regression is demonstrated in Figure 3, which shows that the three regions with higher intermodel standard deviation (IMSTD) in zonal mean temperature are the areas where ΔT300, ΔAMPL, and ΔSUA have the largest influence. Since ΔSUA is not strongly correlated with the other two changes (while the ΔT300 and ΔAMPL are significantly correlated, corr = 0.57, with each other, when calculated directly from the original fields), removing the tropical and polar signals does not strongly affect the ΔSUA regression patterns. Nevertheless, we choose this approach because it guarantees that the tropical and polar signals do not alias to the ΔSUA patterns. Also, we find it interesting to contrast ΔSUA patterns with those from regressing on the other two considered changes.

©2014. American Geophysical Union. All Rights Reserved.

2.2. Time-Lagged Correlation From October to March

A time-lagged correlation is carried out by correlating the February surface Northern Annular Mode (NAM) change (defined below) with the October to March monthly mean zonal mean zonal wind changes, across all available models. Prior to the time-lagged correlation, a sequential linear regression (in a similar fashion as in the previous subsection, but for each month separately) is applied to the zonally and monthly averaged zonal winds and SLP, first regressing on the ΔT300 and then the ΔAMPL changes across all available models. The time-lagged correlation therefore uses residual fields, and the February NAM is constructed from the SLP residuals.

The time-lagged correlation analysis is inspired by *Kodera et al.* [1990], one of the first who showed that wintertime stratospheric zonal wind anomalies propagate downward and poleward. However, here the analysis is applied across the model responses. February is chosen for the NAM change, following the results by KM12, who showed that the influence of the stratospheric response to $2 \times CO_2$ forcing on the tropospheric circulation maximizes in late winter.

ΔNAM change: ΔNAM is defined as the change in the difference between the 30°–50°N and 60°–90°N averages in zonally averaged SLP fields. ΔNAM is an estimate of the SLP mean change that projects on the pattern of the NAM [*Thompson and Wallace*, 2000; *Baldwin and Thompson*, 2011]. Hence, a positive ΔNAM change so defined indicates a lowering pressure over the Arctic with respect to the middle latitudes, in the SLP change.

3. CMIP5 Versus CMIP3: Response to 1% CO_2 Increase per Year

Zonally averaged zonal wind changes from the 1% CO_2 increase per year simulations are shown in Figures 1a–1c, for the CMIP5 and CMIP3 multimodel ensemble means, and their differences, respectively. Because they are based on 40 year averages, these changes are associated with the transient response to approximately a tripling of CO_2. In the lower-to-middle stratosphere (200–10 hPa) and poleward of 50°N, the wind changes are different in the two multimodel sets. In CMIP3 (Figure 1b), winds strengthen through the stratosphere up to the North Pole, but in CMIP5 (Figure 1a) the strengthening does not extend north of 60°–70°N. The negative change in the high-latitude winds extends throughout the depth of the troposphere and stratosphere in the CMIP5 runs. In contrast, this negative change is limited to the troposphere in the CMIP3 runs. In CMIP5 the zonal wind response is negative poleward of 70°N for at least 66% of the models (light shading, Figure 1a), while it is positive in the stratosphere for the same fraction of models in CMIP3 (light shading, Figure 1b). The CMIP5 − CMIP3 difference (Figure 1c) is characterized by a dipole in the stratosphere, with positive/negative difference equatorward/poleward of 50°N, and differences up to 1 m s^{-1} (comparable to the CMIP3 change in the high-latitude stratosphere). The CMIP5 − CMIP3 difference is significant (at $p < 0.05$ according to a two-tailed *t* test, where *p* is the probability to wrongly reject the null hypothesis of equal responses between CMIP3 and CMIP5) poleward of 60°N from the lower troposphere to the stratosphere. Another small region of significant difference is found in the tropical stratosphere between 30–10 hPa, 10°–20°N. In this region the CMIP5 models consistently simulate a positive response while the response is weaker in the CMIP3 models.

The CMIP5 minus CMIP3 difference in the zonally averaged temperature change (Figure 1d) also shows a dipole in the stratosphere (100–10 hPa), which is consistent with the zonal wind difference (through thermal wind balance): cooling in the low latitudes and warming in the polar region in CMIP5 with respect to CMIP3. In the tropical troposphere, the CMIP5 − CMIP3 temperature difference is less than 0.5 K and not significant, indicating that the average difference in warming (and consequently climate sensitivity) between the two sets of models is small [*Andrews et al*., 2012]. In the Arctic, near-surface warming is significantly larger in the CMIP5 models despite the identical CO_2 forcing. Given the primary role of sea ice loss in the near-surface Arctic warming response [*Screen and Simmonds*, 2010], this increased response in CMIP5 suggests a larger susceptibility of the sea ice model components, associated with advances in the representation and coupling of sea ice processes in CMIP5 with respect to CMIP3 [*Stroeve et al.*, 2012]. A larger near-surface Arctic warming in the CMIP5 models implies, via the thermal wind relation, a larger easterly wind change in the subpolar troposphere in the CMIP5 models [*Woollings*, 2008], as indeed is apparent in Figure 1c. Figure 1c also shows that the easterly wind change differences between the ensembles extends up to 10 hPa. By making use of the sequential regression for future climate projections, in the next section we demonstrate that, while the wind change difference in the troposphere is consistent with the near-surface warming difference, the wind change difference in the polar stratosphere is unlikely to be fully explained by the different near-surface Arctic warming.

©2014. American Geophysical Union. All Rights Reserved.

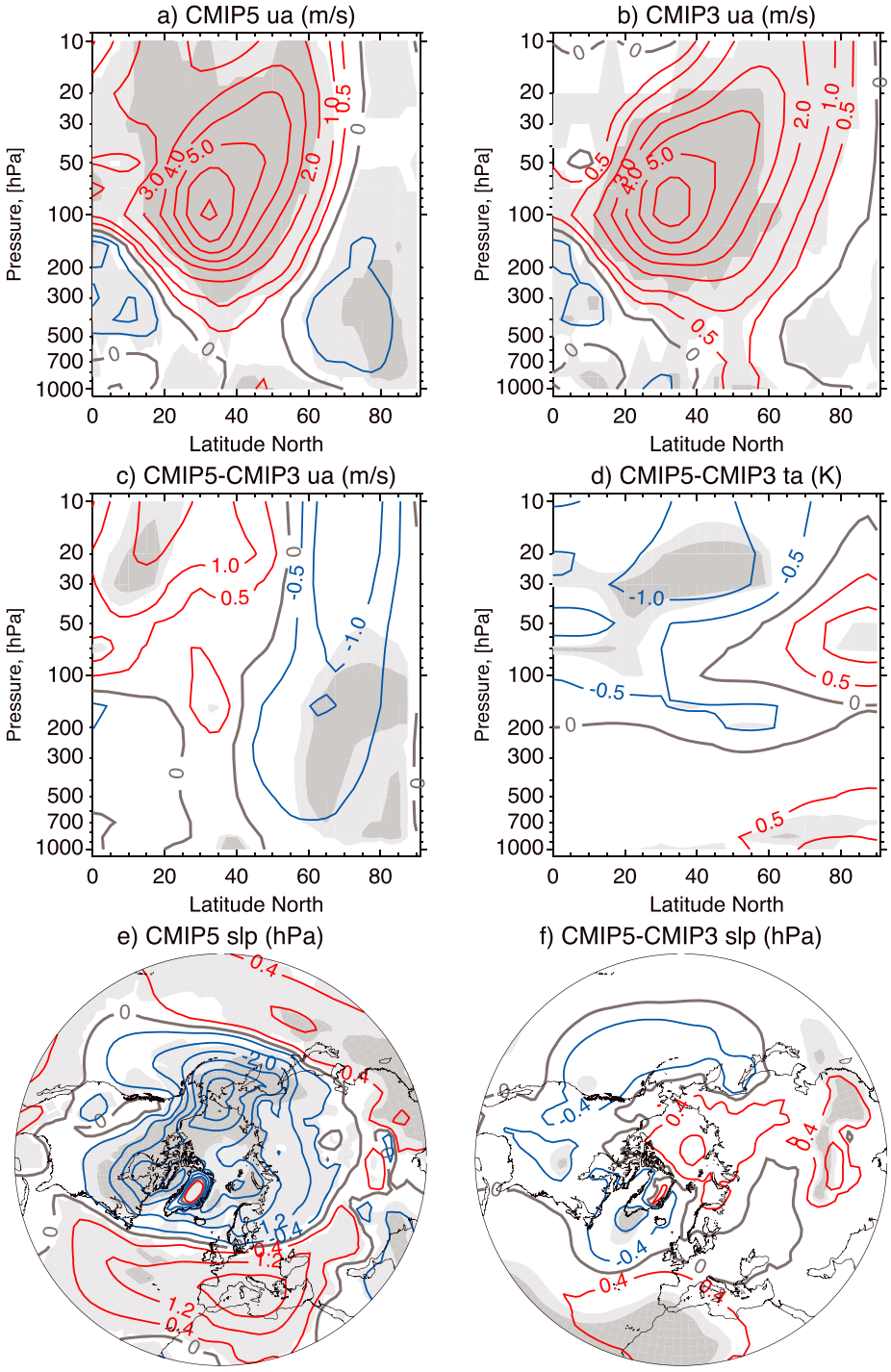

Figure 1. Simulations with 1%yr^{-1} CO_2 increase: DJF change (years 101–140 average minus years 1–40 average) in zonally averaged zonal wind (m s^{-1}) for (a) CMIP5 and (b) CMIP3 multimodel ensembles. CMIP5 minus CMIP3 difference in the DJF changes, for zonally averaged (c) zonal wind (m s^{-1}) and (d) temperature (K). DJF change in PSL (hPa) for (e) CMIP5 multimodel ensemble and (f) CMIP5 minus CMIP3. Contours are drawn for (Figures 1a, 1b, 1c) and (Figure 1d): 0, ±0.5, 1, and then each 1 m s^{-1} and K respectively; for (Figures 1e and 1f): 0, ±0.4, and then each 0.8 hPa. In Figures1a, 1b, and 1e, dark (light) shadings mark areas where 90% (66%) of the models agree on the sign of the change. In Figures 1c, 1d, and 1f, dark (light) shadings mark areas where the differences in the responses are statistically significant according to two-tailed *t* test with $p < 0.05$ (<0.1).

©2014. American Geophysical Union. All Rights Reserved.

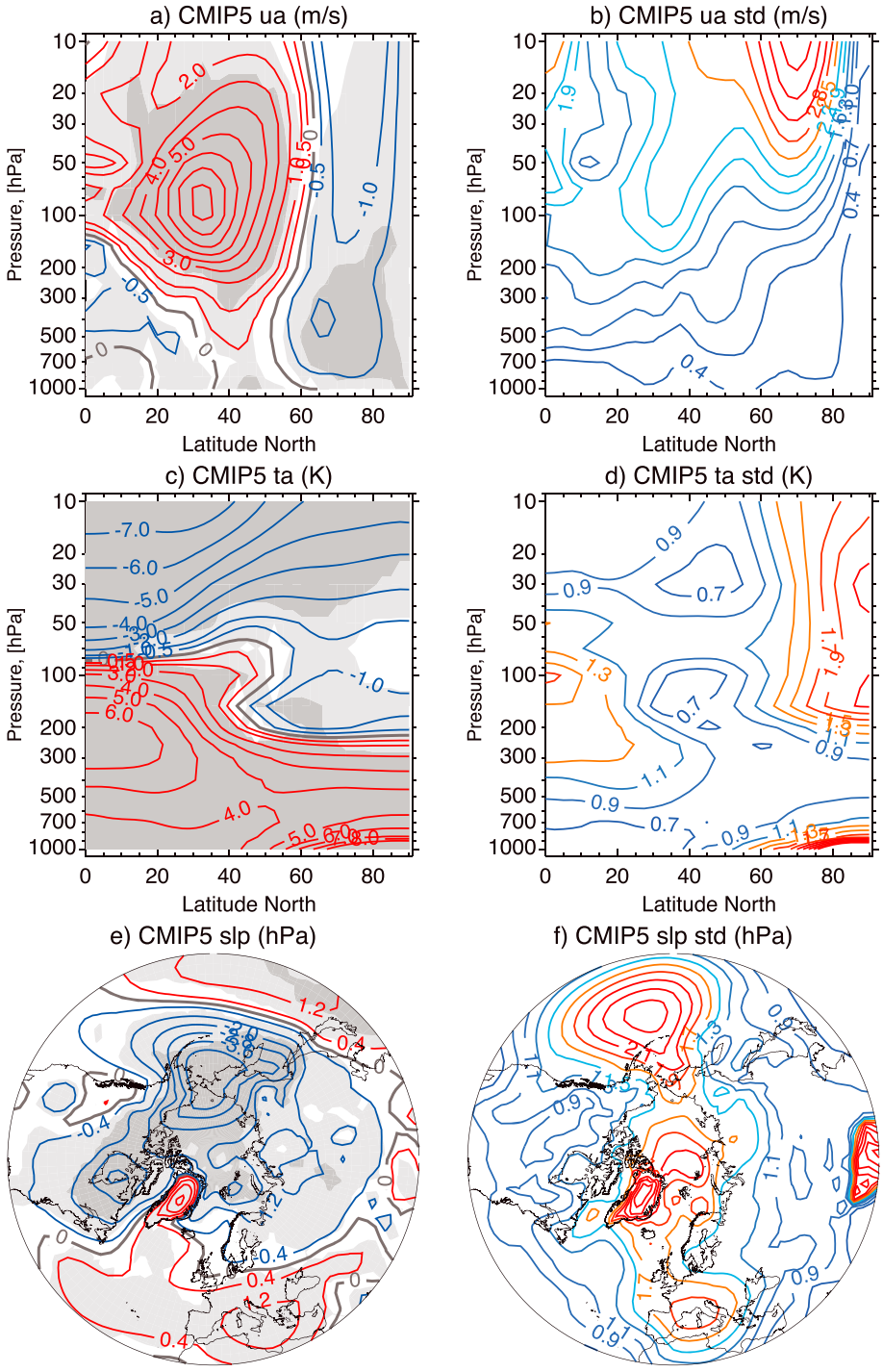

Figure 2. CMIP5 multimodel ensemble, DJF change (2061–2100 RCP8.5 minus 1961–2000 historical). Mean change for (a) zonally averaged zonal wind (m s^{-1}); (c) zonally averaged temperature (K); and (e) PSL (hPa). Intermodel standard deviation of the change for (b) zonally averaged zonal wind (m s^{-1}); (d) zonally averaged temperature (K); and (f) PSL (hPa). Contours are drawn for Figures 2a and 2c: 0, ±0.5, 1, and then each 1 m s^{-1} and K respectively; Figure 2e: 0, ±0.4, and then each 0.8 hPa; Figure 2b: 0.3 m s^{-1}; Figure 2d: 0.2 K; and Figure 2f: 0.2 hPa. In Figures 2a, 2c, and 2e, dark (light) shadings mark areas where 90% (66%) of the models agree on the sign of the change.

©2014. American Geophysical Union. All Rights Reserved.

Figures 1e and 1f show respectively the SLP change in CMIP5 and the CMIP5 − CMIP3 difference in its change. The CMIP5 ensemble SLP change is characterized by the negative changes over the pole and positive changes at midlatitude, as was the case for the CMIP3 models [*Meehl et al*., 2007; *Scaife et al*., 2012]. The difference in SLP change between the CMIP5 and CMIP3 models is not significant in most regions, indicating that the tropospheric circulation response associated with tropical upper tropospheric warming, which is related to climate sensitivity, dominates over other potential influences.

In summary, we find a main difference between the CMIP5 and CMIP3 stratospheric wind response to CO_2, exemplified by the different sign of the response in the high-latitude stratosphere. Albeit small, the easterly change shown in Figure 1a is a novel feature of the CMIP5 multimodel ensemble, not seen in CMIP3 (for previous CMIP3 analysis, see, for instance, *Lorenz and DeWeaver* [2007]). To test the robustness of this result for a larger number of simulations and models, the CMIP5 RCP8.5 future climate projections are analyzed in the next section.

4. CMIP5 RCP8.5 Projections

The CMIP5 RCP8.5 DJF multimodel mean change in zonally averaged stratospheric zonal winds (Figure 2a) shows a dipole pattern, with a negative change at high latitudes (poleward of 60°N) from the surface to the stratosphere. The negative (easterly) change in the polar stratosphere is consistent with the 1% CO_2 increase per year simulations discussed in the previous section (Figure 1a). The stratospheric easterly change shown in Figure 2a is also reproduced (and is about twice as large as that shown in Figure 2a) for a future climate change calculated with respect to the 1861–1900 average of the historical runs (not shown). At low latitudes the winds strengthen around the tropopause, leading to a poleward and upward shift and a strengthening of the subtropical tropospheric jet, as was previously seen in the CMIP3 multimodel mean [*Lorenz and DeWeaver*, 2007]. The negative change poleward of 60°N occurs for at least 66% of the models in the stratosphere 10–100 hPa (light shading, Figure 2a). This level of robustness is similar to that estimated by the 1% CO_2 simulations (Figure 1a) and is also found for a future climate change calculated with respect to the 1861–1900 average.

Changes in zonally averaged air temperature and mean SLP are respectively characterized by the well-known patterns of tropospheric warming and stratospheric cooling (Figure 2c) and decreased/increased SLP over the pole/midlatitudes (Figure 2e). These changes are again consistent with those found in 1% CO_2 increase runs (Figure 1).

Large intermodel standard deviation (IMSTD) indicates the regions where models disagree most (Figure 2, right panels). Given the 40 year averaging and the averaging across multiple realizations (for those models for which more than one realization is available) prior to calculating the changes, it is likely that the spread shown in Figure 2 is dominated by model uncertainty and not internal variability [*Hawkins and Sutton*, 2009]. That this is indeed the case for the spread in the stratospheric winds and the spread in ΔNAM change in SLP is discussed later (Figure 6).

In temperature, three regions of relatively high IMSTD clearly emerge (Figure 2d): the largest IMSTD is at the surface, North Pole, and it is indicative of intermodel differences in the strength of polar amplification, related to sea ice modeling and local feedbacks. This aspect is taken care of in our regression (Figures 3–5) across the model responses by the ΔAMP change. The second largest region of relatively large IMSTD ($>$1 K) is located in the polar stratosphere (north of 60°N). The ΔSUA change by thermal wind balance addresses the potential remote relationships associated with this spread. The third region is in the tropics, 300 to 100 hPa, and it is indicative of intermodel differences in cloud, water vapor/lapse rate feedbacks, causing differences in climate sensitivity [*Bony et al*., 2006]. In the regression, this aspect is encapsulated in the ΔT300 change. IMSTD in SLP (Figure 2f) is largest over the Arctic, the North Pacific Ocean and Central and Southern Europe, excluding regions affected by significant orography (e.g., Greenland and the Himalayas). Sequential regression allows us to make some progress in understanding the large IMSTD in SLP in these regions.

4.1. Sequential Regression

The regression of zonal mean temperature onto the ΔT300 change (Figure 3a) produces a significant positive response throughout the troposphere, indicating that models which produce a stronger upper tropospheric warming in the tropics also warm more throughout the troposphere. This result therefore confirms that the

©2014. American Geophysical Union. All Rights Reserved.

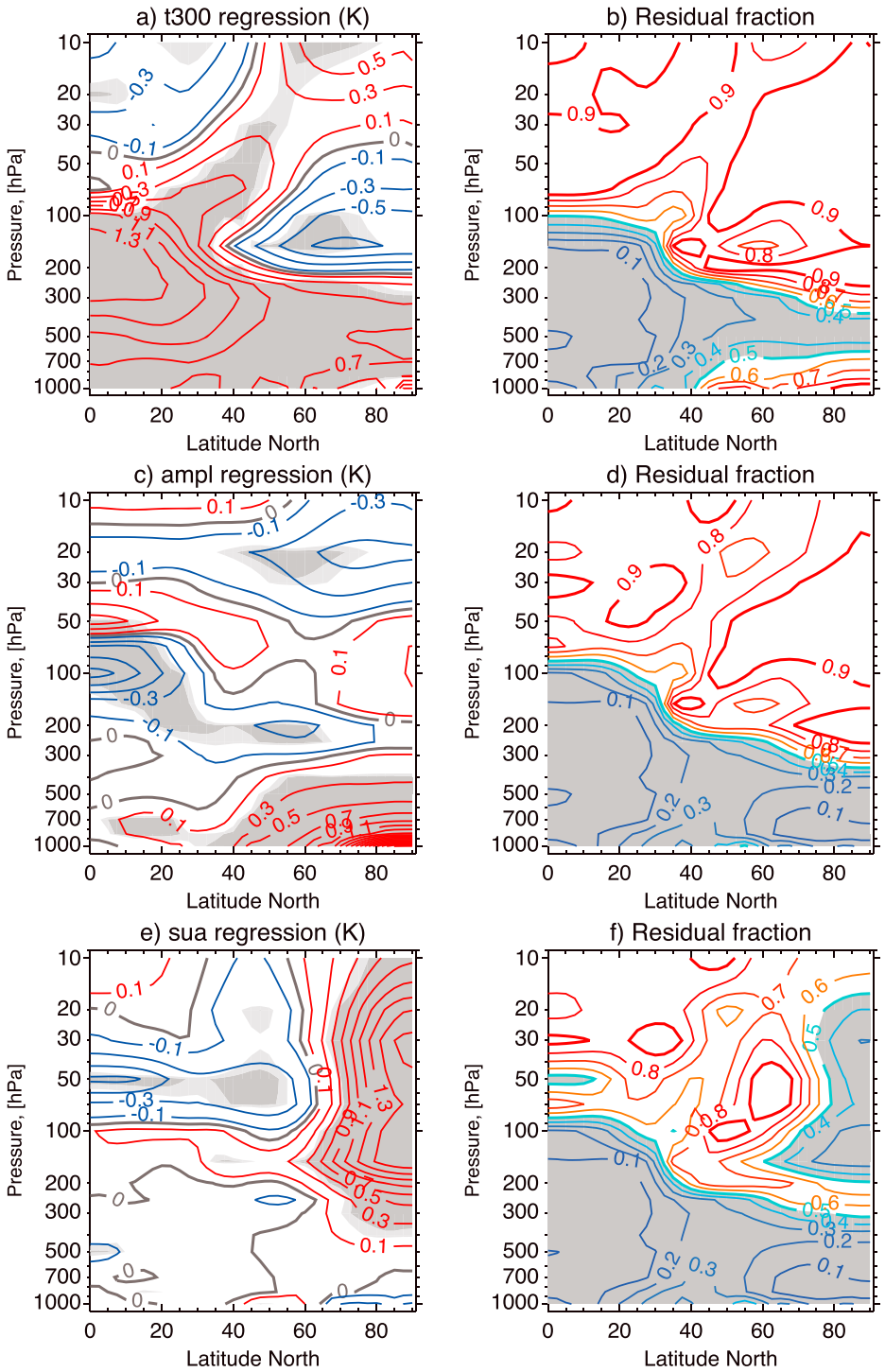

Figure 3. CMIP5 multimodel ensemble, DJF zonally averaged temperature changes (2061–2100 RCP8.5 minus 1961–2000 historical). Regression coefficients (contours: 0, ±0.1, and every 0.2 K thereafter) for (a) ΔT300, (c) ΔAMPL, and (e) ΔSUA. Ratio (contours: 0.1) between the intermodel variance from residuals and that from the total fields, with the residual fields respectively from (b) ΔT300, (d) ΔAMPL, and (f) ΔSUA regressions. In Figures 3a, 3c, and 3e, dark (light) shadings mark areas where the slope of the regression is significantly different from zero according to two-tailed *t* test with $p < 0.05$ (<0.1). In Figures 3b, 3d, and 3f, gray shading indicates ratios less than 0.5.

©2014. American Geophysical Union. All Rights Reserved.

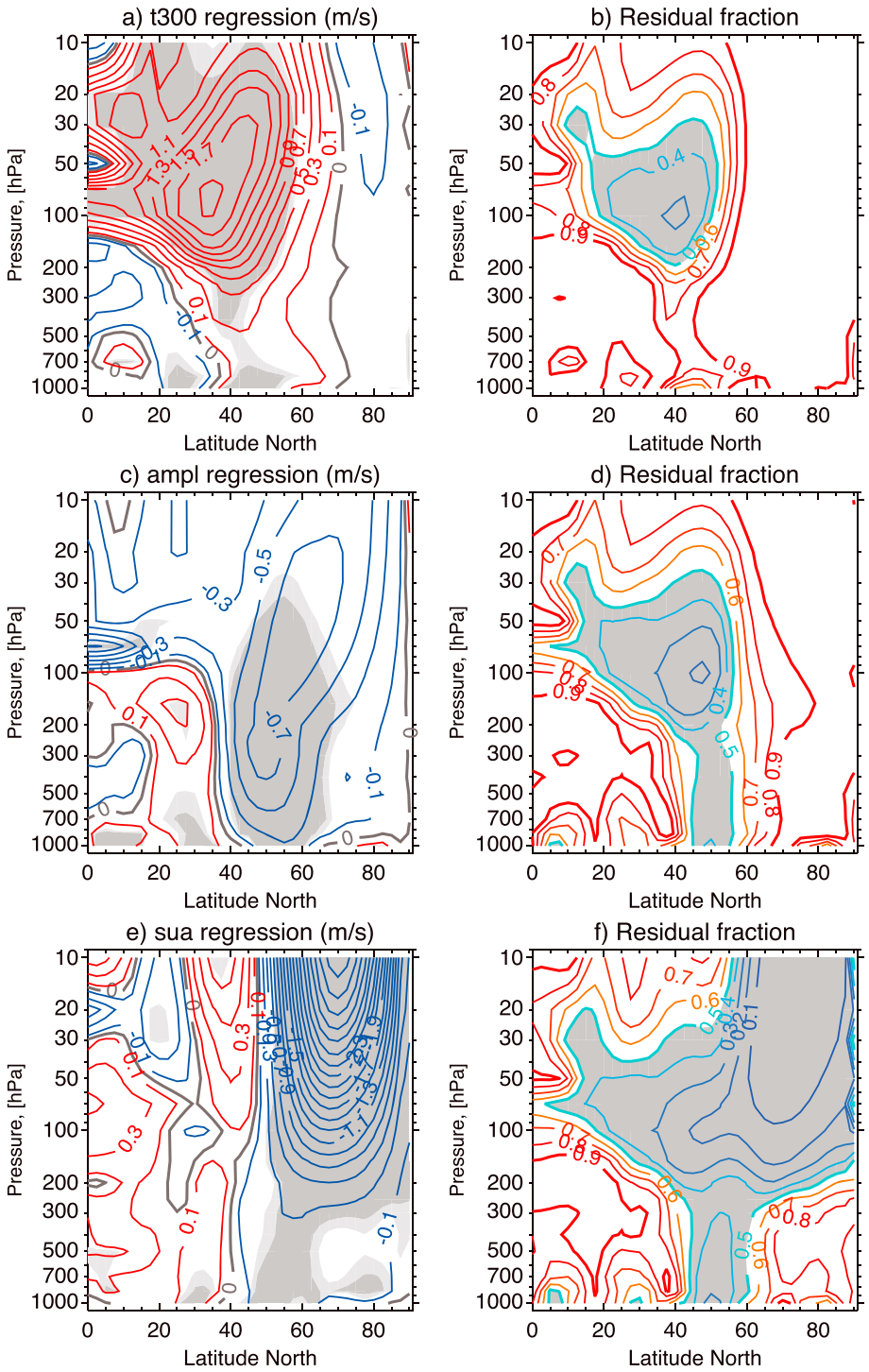

Figure 4. CMIP5 multimodel ensemble, DJF zonally averaged zonal wind change (2061–2100 RCP8.5 minus 1961–2000 historical). Regression coefficients (contours: 0, ±0.1, and every 0.2 m s^{-1} thereafter) for (a) ΔT300, (c) ΔAMPL, and (e) ΔSUA. Ratio (contours: 0.1) between the intermodel variance from residuals and that from the total fields, with the residual fields respectively from (b) ΔT300, (d) ΔAMPL, and (f) ΔSUA regressions. In Figures 4a, 4c, and 4e, dark (light) shadings mark areas where the slope of the regression is significantly different from zero according to two-tailed t test with $p < 0.05$ (<0.1). In Figures 4b, 4d, and 4f, gray shading indicates ratios less than 0.5.

©2014. American Geophysical Union. All Rights Reserved.

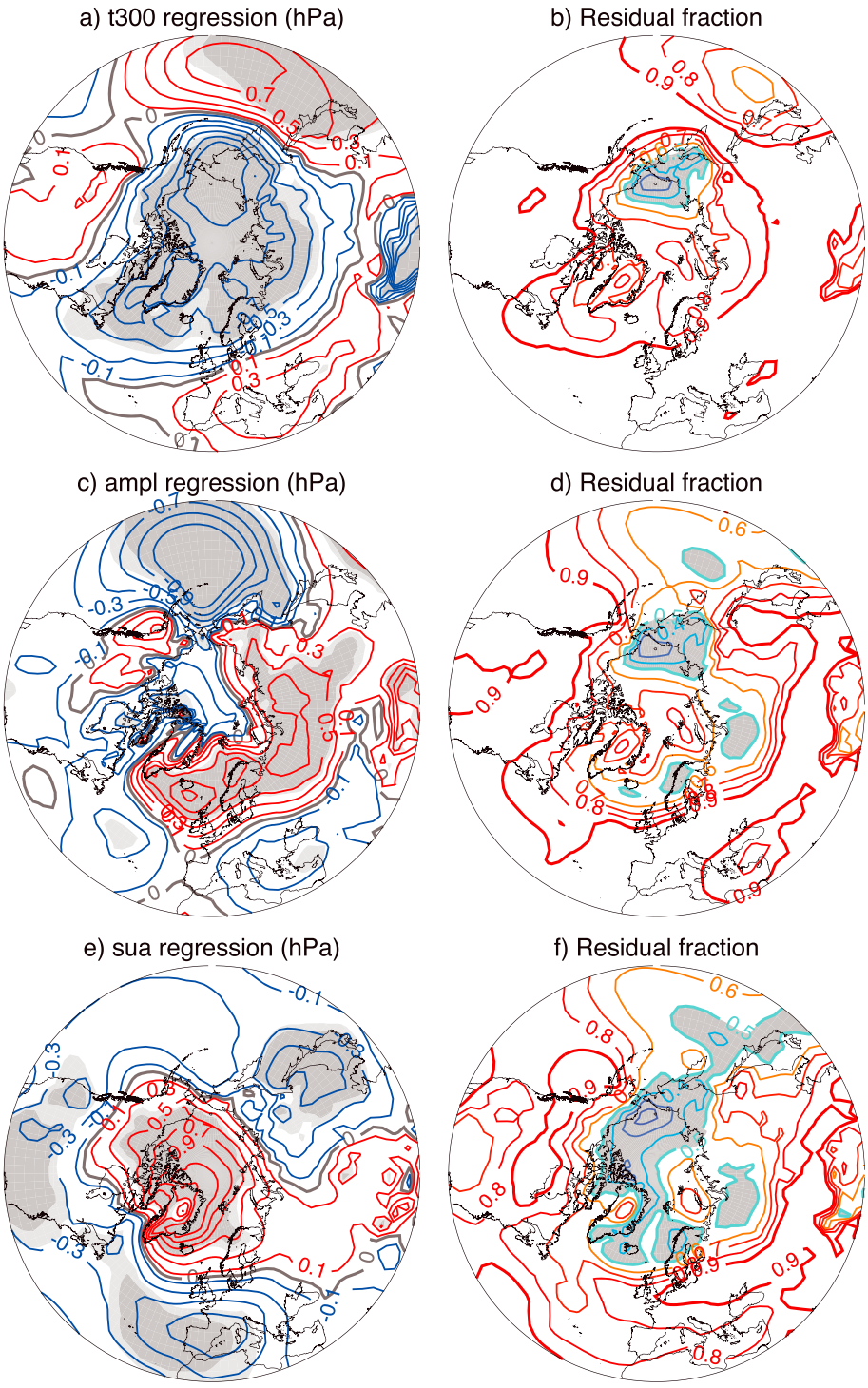

Figure 5. CMIP5 multimodel ensemble, DJF sea level pressure change (2061–2100 RCP8.5 minus 1961–2000 historical). Regression coefficients (contours: 0, ±0.1, and every 0.2 hPa thereafter) for (a) ΔT300, (c) ΔAMPL, and (e) ΔSUA. Ratio (contours: 0.1) between the intermodel variance from residuals and that from the total fields, with the residual fields respectively from (b) ΔT300, (d) ΔAMPL, and (f) ΔSUA regressions. In Figures 5a, 5c, and 5e, dark (light) shadings mark areas where the slope of the regression is significantly different from zero according to two-tailed *t* test with $p < 0.05$ (<0.1). In Figures 5b, 5d, and 5f, gray shading indicates ratios less than 0.5.

©2014. American Geophysical Union. All Rights Reserved.

model spread in the ΔT300 change is linked to differences in surface warming, i.e., climate sensitivity, in the models. The subsequent regression of the ΔT300 residuals onto the ΔAMPL changes (Figure 3c) produces a pattern of strong near-surface warming over the Arctic as expected by the definition of the changes. By showing the ratio between the intermodel variance calculated from the residual fields and that from the total fields (whose square roots are the IMSTD shown in Figure 2), we can depict the degree of success of the regressions in removing the model spread. After the ΔT300 regression, the intermodel variance is substantially reduced (by more than a factor of 2, Figure 3b) in the entire tropical troposphere and in the midtroposphere, 600–400 hPa, at high latitudes). The ΔAMPL regression adds a further reduction (of up to 70–90%) in the near-surface Arctic temperature spread (Figure 3d).

In contrast, the intermodel variance of the stratospheric temperature is unaffected by the ΔT300 and ΔAMPL regressions (Figures 3b and 3d, 100–10 hPa, the ratio remains close to 0.9). The spreads in the stratospheric and tropospheric temperature responses in the CMIP5 models appear therefore to be relatively independent from each other. In the stratosphere, the high-latitude zonal mean temperature relationship to ΔT300 is positive at 10 hPa and negative at ~150 hPa (Figure 2a), suggesting that different processes are diagnosed by the regression. The ΔAMPL regression also shows a secondary negative signal in the tropics (100 hPa, Figure 3c), the origin of which is as yet unknown.

The polar stratospheric temperature intermodel spread is successfully reduced (by more than a factor of 2) after the ΔSUA regression (Figure 3f). A positive and significant relationship between the ΔSUA change and the polar stratospheric temperature is evident (Figure 3e), signaling that weaker zonal winds at 10 hPa are associated with warmer air, by thermal wind balance. The negative ΔSUA regression coefficient in the tropics (50 hPa, Figure 3e) may be related to the link between increased tropical upwelling and a negative change in the stratospheric winds. The increase in tropical upwelling is a typical response of the stratospheric circulation to anthropogenic climate change [*Butchart and Scaife*, 2001; *Butchart et al*., 2006]. Regression coefficients between the tropospheric residuals and ΔSUA are very small.

The results of the ΔT300 regression for the zonally averaged zonal wind and mean SLP changes show that the upper tropospheric warming in the tropics is associated with the strengthening of the subtropical jet, the poleward shift of the extratropical westerlies (Figure 4a), and the decrease in polar SLP (Figure 5a). This result is consistent with *Butler et al.* [2010] who simulated a positive NAM response to the tropical upper tropospheric warming and extends to the Northern Hemisphere the findings of *Arblaster et al.* [2011] who showed that the intermodel spread in the SAM responses is related to the spread in tropical upper tropospheric warming and conforms to the typical tropospheric circulation response associated with climate change [*Meehl et al*., 2007]. A substantial reduction of the intermodel spread is seen across the core of the subtropical jet (Figure 4b). After the ΔAMPL regression, the intermodel variance (Figure 4d) is reduced to less than half and extends to the surface between 40 and 60°N, the latitudes where the ΔAMPL regression coefficient is negative (indicating a reduction in the strength of surface westerlies in response to Arctic amplification) and significant (Figure 4c). Although the ΔAMPL regression coefficient is negative also in the stratosphere, its magnitude is very small (less than a factor of ~5 the magnitude of the ΔSUA regression coefficient, Figure 4e) and not significant.

The intermodel spread in the high-latitude stratospheric winds decreases substantially when regressed against the ΔSUA change (up to 90%, Figure 4f), where, as expected by its definition, the ΔSUA regression coefficient is significant, negative, and large in magnitude (Figure 4e). The ΔSUA regression coefficient is also significant in the troposphere, indicating an equatorward shift of the tropospheric westerlies for a weakening of the high-latitude stratospheric winds. The near-surface strength of the ΔAMPL and ΔSUA relationships is comparable (about $-0.1\ \mathrm{m\,s^{-1}}$, 1000 hPa, Figures 4c and 4e), and the ΔSUA regression further adds to the intermodel spread reduction in the middle high-latitude troposphere. Taken together, these results indicate that uncertainty in both Arctic amplification and stratospheric climate change have equally important effects on future surface circulation.

The regression results for the SLP field (Figure 5) emphasize the difficulty in determining the origin of the uncertainties in the SLP changes. Although the large-scale seesaw pattern associated with the tropical upper tropospheric warming is evident in Figure 5a, with significant ΔT300 regression coefficient over the Arctic (north of 60°N) and the northwest Pacific, the intermodel spread in the midlatitude SLP response is barely reduced after the ΔT300 regression (Figure 5b). In the Arctic, a reduction of generally 20% is found, with only

©2014. American Geophysical Union. All Rights Reserved.

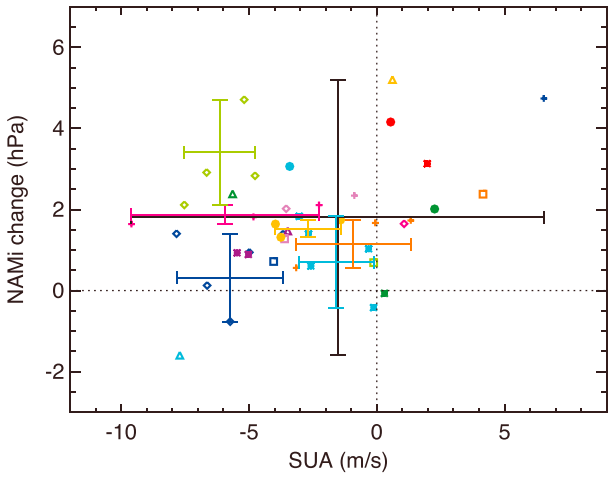

Figure 6. CMPI5 multimodel ensemble, scatter plot of the DJF change (2061–2100 RCP8.5 minus 1961–2000 historical) in the NAM (hPa) and the SUA ($m\,s^{-1}$) changes. Each marker represents a model realization. Multiple realizations from the same model are denoted by the same color. The horizontal and vertical bars denote the respective range of values, by model (in color) and for the whole ensemble set (in black). Correlation (by realization) between the NAM and SUA changes is 0.34 and is significant at $p = 0.025$. The correlation is better for model means and for residuals after ΔT300 and ΔAMPL regressions.

a small region (shaded gray in Figure 5b) showing a substantial reduction in the model spread. The ΔAMPL regression reveals a positive/negative relationship between the Arctic warming and SLP changes in the North Atlantic and Siberian region/North Pacific. Although the ΔAMPL response projects on the zonal mean changes (Figure 4c), Figure 5c shows that the response has a large nonzonal component. After the ΔAMPL regression (Figure 5d), intermodel spread is reduced mostly around the central Arctic: over Siberia, Northern Scandinavia, and Northern Atlantic.

Throughout most of the Arctic, the intermodel spread of SLP is reduced to about half, after the ΔSUA regression (Figure 5f), which also contributes to some intermodel spread reduction at midlatitudes (e.g., 0.8 contour over the Atlantic and South Europe. Overall, however, the relatively small reduction of the intermodel spread in the midlatitude SLP response indicates that other factors not accounted for by our regression analysis (including internal variability and ocean-atmosphere coupling [*Woollings et al.*, 2012]) may contribute to tropospheric circulation changes in the Atlantic-Eurasia region and also North America.

The uncertainty in the SLP changes in the Arctic region (poleward of 60°N) appears therefore to primarily be a combination of tropical upper tropospheric warming (−0.5 to −0.9 hPa response to a unit change in ΔT300, poleward of 60°N, Figure 5a) and stratospheric changes (0.5 to 1 hPa response to a unit change in ΔSUA, poleward of 70°N, Figure 5e). Figures 4e and 5e suggest a sensitivity of almost 1 hPa Arctic SLP mean change per ~3.5 $m\,s^{-1}$ high-latitude stratospheric mean wind change at 10 hPa.

On hemispheric scale, the SLP change pattern revealed by the ΔSUA regression (Figure 5e) is reminiscent of the NAM of variability [*Thompson and Wallace*, 2000], especially in the North Atlantic and European sector, and also of the typical patterns of tropospheric anomalies following stratospheric sudden warmings [*Limpasuvan et al.*, 2004; *Charlton and Polvani*, 2007]. Since NAM is a mode of internal variability, it is therefore possible that the intermodel spread in both ΔSUA and SLP changes is merely an indicator of internal model variability, instead of intermodel disagreement. We test the contribution of the internal variability to the spread in simulated ΔSUA and ΔNAM responses by comparing the spread across multiple realizations of the same model to the total spread in simulated responses. Figure 6 shows a scatter plot of the ΔSUA change (in $m\,s^{-1}$ and without sign reversal) and the SLP based ΔNAM change (in hPa), both calculated from the original DJF mean fields without any regression. Figure 6 clearly shows that the ΔSUA intermodel spread is larger (with a range from −10 to +7 $m\,s^{-1}$) than the interrealization spread by model. Following *Karpechko* [2010] we apply the analysis of variance test to separate the contributions of the intermodel and intramodel spreads to the total variance of the ΔSUA and ΔNAM changes. The calculations show that the intermodel variances in ΔSUA (18.2 m^2s^{-2}), and ΔNAM (3.0 hPa^2) significantly exceed the mean intramodel variances (3.6 m^2s^{-2} and 0.6 hPa^2 respectively). In both cases the ratio of the intermodel to intramodel variance (*F* statistics) is close to 5, indicating that the two variances are statistically different ($p < 0.05$) using an *F* test. This result indicated that the intermodel spread dominates over the intramodel spread (internal variability) for the model ensemble used.

4.2. Time-Lagged Correlation and Seasonality of the Changes

KM12 showed that the early winter stratospheric easterly response to $2 \times CO_2$ forcing slowly progresses downward, so that the stratospheric influence on the tropospheric circulation maximizes in late winter (their Figures 8, 9, and 10). Here we ask if a similar seasonal dependence can be diagnosed from the CMIP5

©2014. American Geophysical Union. All Rights Reserved.

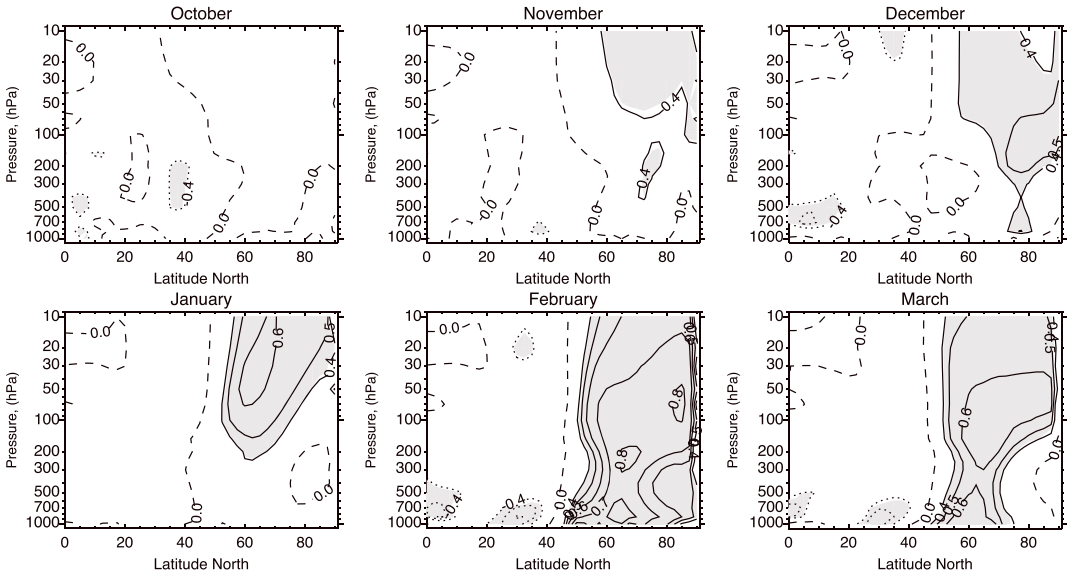

Figure 7. CMIP5 multimodel ensemble, change (2061–2100 RCP8.5 minus 1961–2000 historical). Correlation between the February ΔNAM change and the monthly and zonally averaged zonal wind changes, October to March. Gray shading indicates statistical significant correlation with $p > 0.05$. The correlation is calculated on residual fields, after ΔT300 and ΔAMPL regressions.

multimodel ensemble and so test the hypothesis that the uncertainty in the tropospheric response correlated with the ΔSUA (zonally averaged) change originates from the stratosphere. The surface response is diagnosed using the February ΔNAM change in SLP (see section 2). This February ΔNAM change is thereafter correlated with the monthly and zonally averaged zonal wind change at each grid point, from October to March. Significant instantaneous (February) and forward (March) correlations range from the surface to 10 hPa. Significant backward correlations (January to November) are located in the stratosphere, poleward of ~60°N. Positive correlations are consistent with our current view of stratosphere-troposphere dynamical coupling, which associates weak/strong stratospheric winds with negative/positive surface ΔNAM, with a time lag of several weeks. Given that ΔNAM correlates with the high-latitude stratospheric winds for negative lags, Figure 7 indicates that at least part of the February ΔNAM change (which uncertainty is dominated by intermodel spread, as in the case of its December to February (DJF) mean, Figure 6) seen in the CMIP5 RCP8.5 projections is associated with stratospheric wind changes earlier in winter. The consistency between these results and those from the controlled experiments by KM12 provides support for a stratosphere to troposphere direction in the DJF ΔSUA and SLP relationship found in Figure 5.

The stratospheric zonally averaged zonal wind response (prior to any regression) also shows a seasonality in the polar regions, with the negative change developing from December to January and decaying from March to April (not shown). Consistent with the loss of signal by April, no difference in final warming date occurs. An analysis of the response of the timing of the stratospheric final warming (following the methods of *Black et al.* [2006]) has shown that while the CMIP5 models are able to represent the salient characteristics of the stratospheric final warming events in the troposphere and stratosphere, there is no discernible change in the timing and behavior of these events between the historical and RCP8.5 model ensembles (not shown).

The seasonality of the stratospheric circulation change can be shown by diagnosing tropical upwelling at 70 hPa (Figure 8). First, Figure 8 confirms that for the available CMIP5 models, tropical upwelling is increased in response to anthropogenic climate change, as previously reported in climate models that extend into the upper atmosphere [e.g., *Butchart and Scaife*, 2001; *Butchart et al.*, 2006], as well as in an atmospheric model with a top at 10 hPa by KM12. Second, Figure 8 shows that November–December is the season when a sharp increase in the tropical upwelling occurs.

Although an increase in tropical upwelling in the lower stratosphere does not necessarily imply an increase in downwelling in the polar region, the majority of the models show an increased downwelling

©2014. American Geophysical Union. All Rights Reserved.

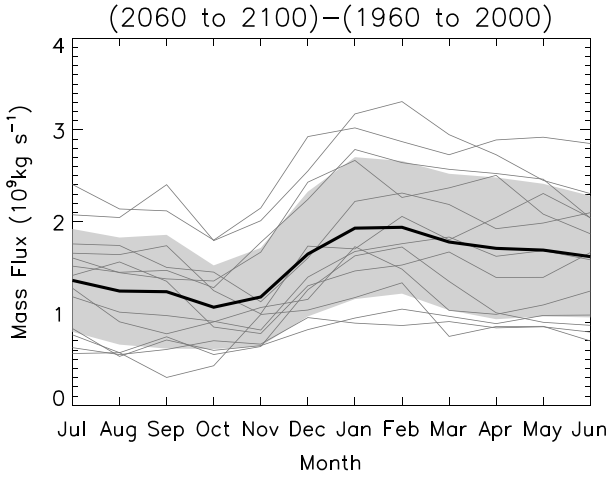

Figure 8. CMIP5 multimodel ensemble, monthly mean change (2060–2100 RCP8.5 minus 1960–2000 historical) in total mass upwelling (10^9 kgs^{-1}) between turn around latitudes at 70 hPa from July to June. The thick solid curve shows the multimodel mean change, and the thin gray curves are the changes by model. Shading indicates 1 intermodel standard deviation.

in the polar stratosphere from autumn to midwinter (January) and for a deep layer of the stratosphere, 100–10 hPa (shaded regions of Figure 9b). In the lower stratosphere (50 hPa), November–December is also the time when increased downwelling is not restricted to the polar region, but extends to 40°N, while increased upwelling is found across the entire tropics (Figure 9d). In summary, Figures 8 and 9 provide evidence that in late autumn and early winter, the increase in the Brewer-Dobson circulation (BDC) extends to the polar region, thus with the potential to lead to the weakening of the high-latitude stratospheric winds shown in Figure 2a. For further analysis of the BDC in the CMIP5 models, see *Hardiman et al.* [2013].

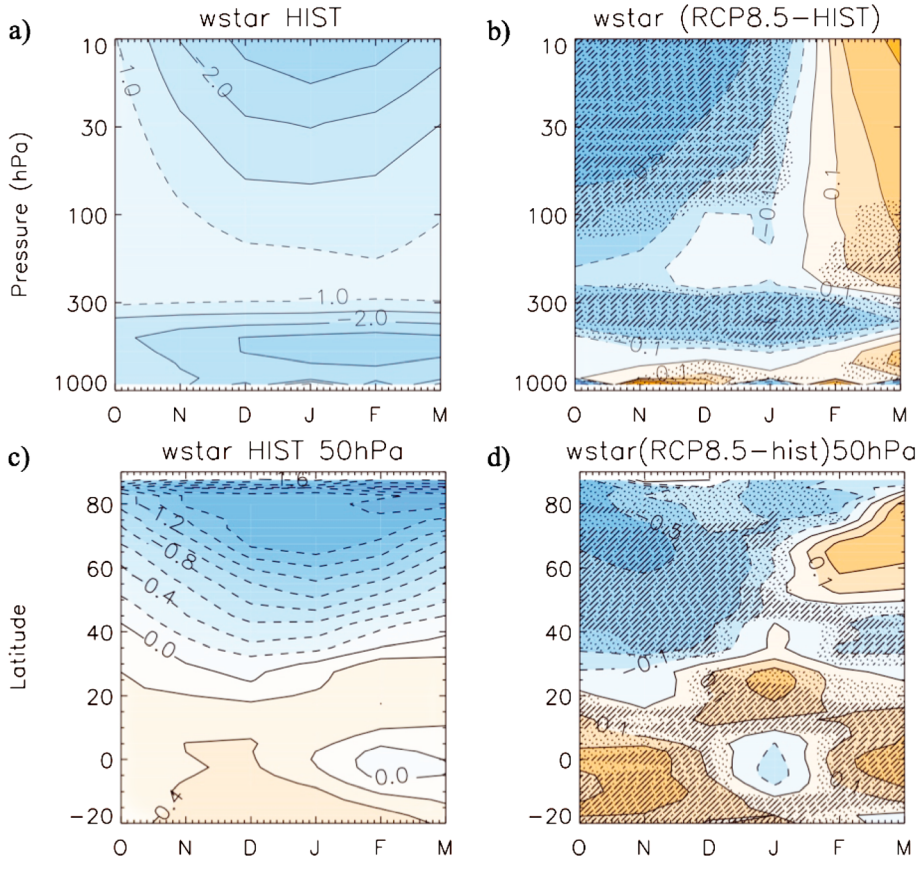

Figure 9. CMIP5 multimodel ensemble, residual vertical velocity (mm s^{-1}). Historical multimodel mean (1961–2000) from October to March for (a) area-weighted average poleward of 60°N and (c) section at 50 hPa. Multimodel mean change (2061–2100 RCP8.5 minus 1961–2000 historical) for (b) area-weighted average poleward of 60°N and (d) section at 50 hPa. Contours are drawn for (Figure 9a) 0.5 mm s^{-1}; (Figure 9c) 0.2 mm s^{-1}; and for (Figures 9b and 9d): 0, ±0.1, 0.2, 0.5, 0.7, … mm s^{-1}. Stripe (dot) shadings mark areas where 90% (66%) of the models agree on the sign of the change.

©2014. American Geophysical Union. All Rights Reserved.

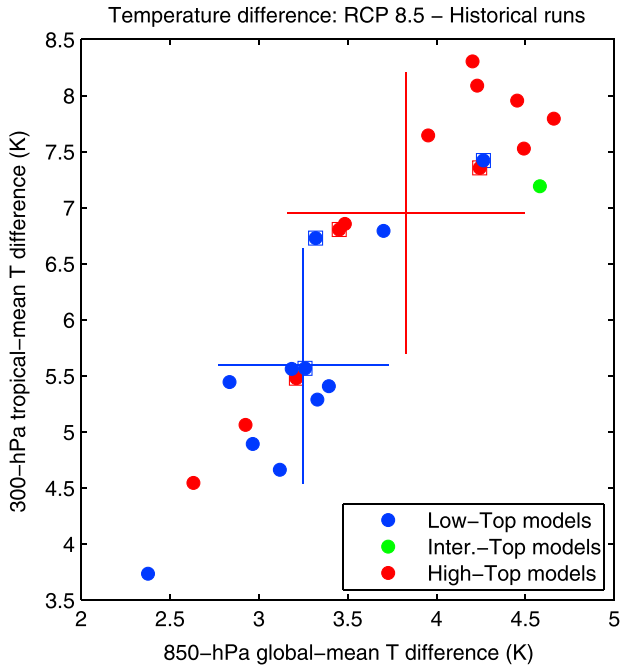

Figure 10. CMIP5 multimodel ensemble, change (2061–2100 RCP8.5 minus 1961–2000 historical). Scatter plot of tropical (30°S–30°N) annual mean temperature change at 300 hPa and global annual mean temperature change at 850 hPa. Each marker represents a model, high top models in red and low top models in blue. One model (green) is labeled intermediate. High/low top model "pairs" (see text) shown by squares.

5. Unreliability of a High and Low Top Subdivision for the CMIP5 Multimodel Ensemble

McLandress et al. [2012] and *Previdi and Polvani* [2012] have recently warned of the potential problems and ambiguities that can arise from interpreting climate change in subsets of CMIP ensembles. Here we test the feasibility of the subdivision of the CMIP5 ensemble of models according to the location of the model top (*Charlton-Perez et al.* [2013], high top models are those with lids at pressures $<$ 1 hPa, intermediate is a model with top at 1 hPa, the rest are low top models) for analysis of future projection of climate change. Near the surface (850 hPa, *x* axis in Figure 10), the majority of the high top models (red markers) and the intermediate model (green marker) are warming more than the majority of the low top models (blue markers). The spread in near-surface global warming (slightly more than 2 K) as depicted in Figure 10 is a signal of intermodel difference in climate sensitivity [*Bony et al.*, 2006]. Intermodel difference in climate sensitivity in the CMIP5 multimodel ensemble is similar to previous estimates [*Andrews et al.*, 2012]. The difference in near-surface warming between the two CMIP5 subsets is substantial (~0.7 K) and translates to an even larger difference (between 1 and 1.5 K) in upper troposphere tropical temperature change (300 hPa, *y* axis in Figure 10), because the tropical troposphere response to the radiative forcing of an increase in CO_2 follows the moist adiabatic decrease of temperature with elevation (e.g., lapse rate, see *Bony et al.* [2006] for a review). These results are relevant to the intermodel spread in circulation changes, because the warming of the tropical upper troposphere is a key driver of the tropospheric circulation changes leading to high latitude SLP changes (Figure 5a). The difference between the high and low top models related to their climate sensitivity is therefore likely to dominate differences in their predictions of future high-latitude circulation change. Intermodel differences in climate sensitivity are dominated by differences in radiative feedback and ocean heat uptake impacts (e.g., *Bony et al.* [2006]; *Dufresne and Bony* [2008], and for an analysis using the CMIP5 ensemble of models, see *Andrews et al.* [2012]). There is no theoretical evidence to implicate stratospheric processes in intermodel differences in climate sensitivity; therefore, we conclude that to subdivide the CMIP5 set in the high and low top model subensembles, to detect the stratospheric response to climate change and its potential remote influences, is an unreliable method that can lead to spurious results. Note as well that three pairs of models that are very closely related and differ mostly (but not only) in their model top location

©2014. American Geophysical Union. All Rights Reserved.

(highlighted by squares in Figure 10) have virtually the same tropospheric warming, supporting our conclusion that global surface warming is unrelated to stratospheric processes.

6. Discussion and Conclusions

We have evaluated future projection of northern winter stratospheric mean changes by the CMIP5 RCP8.5 scenario and compared CMIP5 and CMIP3 idealized projections with CO_2 increasing 1% per year. The main results for stratospheric mean changes and stratosphere-troposphere coupling follow, and we conclude with final remarks.

6.1. Stratospheric Mean Changes

The main findings on DJF stratospheric mean changes in CMIP5 are as follows:

1. In the stratosphere, a robust easterly change in the zonally averaged zonal winds is found (Figures 1 and 2). This stratospheric easterly change contrasts with the westerly change simulated by the CMIP3 models.
2. The uncertainty in the stratospheric mean change is comparable in the RCP8.5 and 1% CO_2 increase per year simulations. In both cases, about 70% of the models show the easterly change (Figures 1a and 2a). The same uncertainty is also found for a future RCP8.5 climate change calculated with respect to the 1861–1900 average of the historical runs. Although we can thus conclude that the majority of the models show the easterly change, the intermodel spread, even in the sign of this change, is not negligible.
3. The uncertainty in the stratospheric change is likely due to structural differences in models. In the available runs, internal variability does not play a dominant role, because the intermodel spread is larger than the intramodel spread (Figure 6).
4. For all the available CMIP5 models, tropical upwelling is found to increase (Figure 8), generalizing previously reported results for climate models that extend into the upper atmosphere. In late autumn and early winter, the increase in the BDC extends to the polar region, thus with the potential to lead to the weakening of the high-latitude stratospheric zonally averaged winds (Figure 9).

6.2. Stratosphere-Troposphere Coupling

The main results on stratosphere-troposphere coupling in CMIP5 are as follows:

1. Reducing the uncertainty in stratospheric zonally averaged change may effectively narrow the uncertainty in DJF SLP change. The relationship between the easterly change of the high-latitude stratospheric winds (i.e., the ΔSUA change) and the SLP change projects on the negative phase of the NAM (Figure 5e), in agreement with previous works. The size of this effect (Figures 5e and 5f) is such that reducing the spread of future projections of stratospheric changes would likely be as effective as reducing the spread in climate sensitivity in models.
2. The coupling between zonally averaged zonal wind and SLP changes shows a distinct seasonal progression (Figure 7). The surface NAM response in February is at least partially associated with stratospheric wind changes in February and earlier in winter (i.e., backward in time till December and even November). The overall consistency of the seasonal progression in the time-lagged correlation between high-latitude stratospheric winds and SLP changes, with the results from the controlled experiments by *Karpechko and Manzini* [2012], provides support for a stratosphere to troposphere coupling of the zonally averaged changes.
3. The uncertainty in the middle high-latitude tropospheric DJF easterly change is related to the intermodel spread in the tropospheric circulation response to both polar amplification and the stratospheric circulation changes (Figures 4c–4f). In the troposphere, ΔSUA and polar amplification seem to have impacts of similar overall magnitudes, but in some regions the impact of ΔSUA is larger and in others the impact of ΔAMPL is larger.

On methods for diagnosing stratosphere-troposphere coupling, we found that the high/low top subdivision of the CMIP5 ensemble is characterized by a substantial difference in global surface warming. Therefore, this subdivision is easily dominated by intermodel differences related to climate sensitivity. A too small sample of models and too many model interdependencies (e.g., use of similar parameterizations or model components) are plausible reasons for this spurious result (on the effective number of independent models in CMIP, see *Pennell and Reichler* [2011] and *Knutti et al.* [2013]). The investigation of these questions is outside the scope of this work.

©2014. American Geophysical Union. All Rights Reserved.

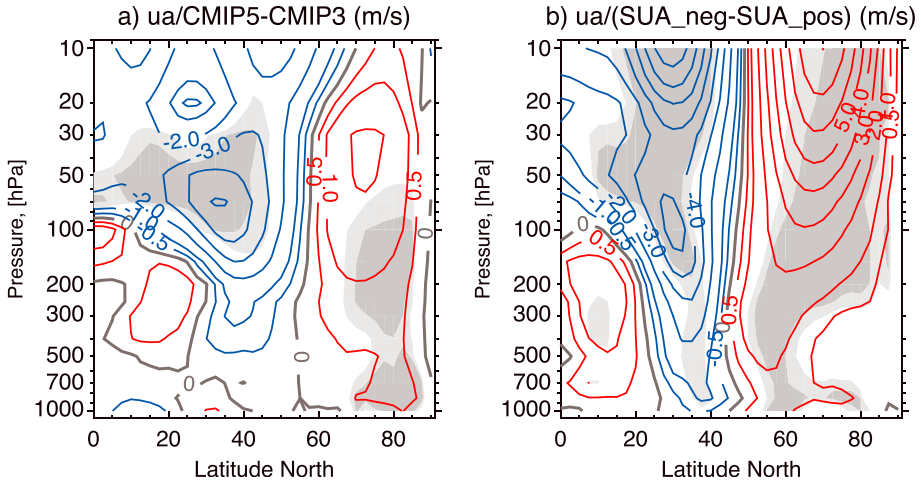

Figure 11. DJF zonally averaged zonal wind (m s^{-1}): (a) difference CMIP5 minus CMIP3, for the years 1–40 average of the 1% yr^{-1} CO_2 increase simulations and (b) difference CMIP5 SUA_neg minus CMIP5 SUA_pos subgroups, for the years 1961–2000 average of the historical simulations. The SUA_neg and SUA_pos model ensembles group the CMIP5 models according to their response in the stratosphere: The SUA_neg/SUA_pos models have negative/positive zonally averaged zonal wind change at 10 hPa, 70–80°N. Contours in Figures 11a and 11b are 0, ±0.5, 1, and then each 1 m s^{-1}. Dark (light) shadings mark areas where the differences are statistically significant according to two-tailed t test with $p < 0.05$ (<0.1).

6.3. Final Remarks

As with all studies of the CMIP5 ensemble, a caveat on our analysis is the relative low number of model available with multiple future realizations, to compare intermodel and intramodel spread. In the available runs, internal variability does not play a dominant role, possibly because of the 40 year averages considered. To advance on our understanding of the role of stratospheric changes for future climate, it would be of interest if future coordinated climate projection experiments placed more emphasis on the number of realizations by each model, in contrast to the number of future scenarios.

The origin of the stratospheric zonally averaged change and its spread is still an open question. The comparison with CMIP3 suggests that model differences related to how the stratosphere is resolved (including wave-mean flow interaction, damping of resolved waves, and gravity wave parameterizations) are implicated, because of the larger number of high top models in CMIP5. Model differences in the lower stratospheric climatological mean state could be relevant [*Sigmond and Scinocca*, 2010]. In this regard, we note that with respect to CMIP3, the CMIP5 models have weaker climatological mean westerlies in the lower stratosphere near the upper flank of the tropospheric jet, 100–50 hPa, 30°N–50°N, (Figure 11a) and that a similar difference in climatological mean westerlies is found by compositing the CMIP5 models according to their high-latitude stratospheric wind changes (e.g., compositing by ΔSUA, Figure 11b). Although Figure 11 shows significant differences in other regions, the lower midlatitude stratosphere can be most relevant (J. F. Scinocca and M. Sigmond, personal communication, 2014) in setting the planetary wave propagation characteristics of the climatological mean state, which in turn can condition the flow toward different responses in the high-latitude stratospheric zonally averaged change, as explained in *Sigmond and Scinocca* [2010]. Figure 11 therefore provides support for a role of the *Sigmond and Scinocca* [2010] mechanism in explaining the spread in ΔSUA, although the climatological wind differences shown in Figure 11 are not necessarily due to orographic gravity wave drag parameterizations, as in *Sigmond and Scinocca* [2010].

Relative to the CMIP3 models, the CMIP5 models include additional advances also in the representation of other components of the climate and Earth system, notably in how sea ice processes are treated. Further research is therefore needed to better understand the lagged nature of the stratosphere-troposphere coupling. Specifically, how changes in the climate system (including ocean, sea ice, and tropospheric circulation changes) affect the stratospheric response in late autumn and early winter, prior to a downward coupling in late winter. Further research is needed also to discriminate among the proposed mechanisms of downward coupling [e.g., *Ambaum and Hoskins*, 2002; *Kushner and Polvani*, 2004; *Song and Robinson*, 2004; *Thompson et al.*, 2006], a topic outside the scope of this work.

©2014. American Geophysical Union. All Rights Reserved.

In summary, our study supports conclusions from previous work that stratosphere-troposphere coupling can be an important factor in determining future changes in the tropospheric circulation response. Since anticipating regional climate and circulation changes is a key challenge for climate prediction, our findings add motivation to the call for a better understanding of the relative roles and interdependence of stratospheric processes, lower atmosphere and ocean circulations, and sea ice processes.

Acknowledgments

We acknowledge the World Climate Research Programme's Working Group on Coupled Modelling, which is responsible for CMIP, and we thank the climate modeling groups for producing and making available their model output. For CMIP the U.S. Department of Energy's Program for Climate Model Diagnosis and Intercomparison provides coordinating support and led development of software infrastructure in partnership with the Global Organization for Earth System Science Portals. We are grateful to Thomas Birner and Lorenzo Polvani for providing comments to an earlier version of the manuscript. Evgeny Volodin, John Wilson, and Seiji Yukimoto are kindly acknowledged to have provided the residual vertical velocity diagnostic. We thank Judith Perlwitz, John Scinocca, Michael Sigmond, Hauke Schmidt, and the anonymous reviewers for their constructive reviews and suggestions. E.M. and S.C.H. were partially supported by the EC COMBINE project (GA 226520). A.Y.K. was funded by the Academy of Finland, grant 259537. A.A.S. and S.C.H. were supported by the Joint DECC/Defra Met Office Hadley Centre Climate Programme (GA01101). M.P.B. was funded by NSF under the U.S. CLIVAR program and the Office of Polar Programs. The research efforts of R.X.B., B.A.M., and Y.-Y.L. were supported by the Office of Science (BER) of the U.S. Department of Energy and by the National Science Foundation grant, ARC-1107384. J.A. and L.J.G. were funded by the UK Natural Environment Research Council (NERC) and National Centre for Atmospheric Science (NCAS). S.W.S. was funded by the Korea Meteorological Administration Research and Development Program under grant CATER 2012-3065. E.P.G. was supported by the U.S. NSF, grant AGS-1264195. NCAR is sponsored by the National Science Foundation. N.C. was supported by the Spanish Ministry of Science and Innovation (MCINN) through the MATRES (CGL2012-34221). G.Z. was funded by NERC under the TEMPEST project.

References

Ambaum, M. H. P., and B. J. Hoskins (2002), The NAO troposphere–stratosphere connection, *J. Clim.*, *15*, 1969–1978.

Andrews, T., J. M. Gregory, M. J. Webb, and K. E. Taylor (2012), Forcing, feedbacks and climate sensitivity in CMIP5 coupled atmosphere-ocean climate models, *Geophys. Res. Lett.*, *39*, L09712, doi:10.1029/2012GL051607.

Arblaster, J. M., G. A. Meehl, and D. J. Karoly (2011), Future climate change in the Southern Hemisphere: Competing effects of ozone and greenhouse gases, *Geophys. Res. Lett.*, *38*, L02701, doi:10.1029/2010GL045384.

Baldwin, M. P., and T. J. Dunkerton (2001), Stratospheric harbingers of anomalous weather regimes, *Science*, *294*, 581–584.

Baldwin, M. P., and D. W. J. Thompson (2011), A critical comparison of stratosphere–troposphere coupling indices, *Q. J. R. Meteorol. Soc.*, *135*, 1661–1672.

Black, R. X., B. A. McDaniel, and W. A. Robinson (2006), Stratosphere-troposphere coupling during spring onset, *J. Clim.*, *19*, 4891–4901.

Bony, S., et al. (2006), How well do we understand and evaluate climate change feedback processes?, *J. Clim.*, *19*, 3445–3482.

Butchart, N., and A. A. Scaife (2001), Removal of chlorofluorocarbons by increased mass exchange between the stratosphere and troposphere in a changing climate, *Nature*, *410*, 799–802.

Butchart, N., et al. (2006), Simulations of anthropogenic change in the strength of the Brewer-Dobson circulation, *Clim. Dyn.*, *27*, 727–741, doi:10.1007/s00382-006-0162-4.

Butler, A. H., D. W. J. Thompson, and R. Heikes (2010), The steady-state atmospheric circulation response to climate change-like thermal forcings in a simple general circulation model, *J. Clim.*, *23*(13), 3474–3496, doi:10.1175/2010JCLI3228.1.

Cagnazzo, C., and E. Manzini (2009), Impact of the stratosphere on the winter tropospheric teleconnections between ENSO and the North Atlantic and European Region, *J. Clim.*, *22*, 1223–1238, doi:10.1175/2008JCLI2549.1.

Charlton, A. J., and L. M. Polvani (2007), A new look at stratospheric sudden warmings. Part I: Climatology and modeling benchmarks, *J. Clim.*, *20*, 449–469.

Charlton-Perez, A. J., et al. (2013), On the lack of stratospheric dynamical variability in low-top versions of the CMIP5 models, *J. Geophys. Res. Atmos.*, *118*, 2494–2505, doi:10.1002/jgrd.50125.

Cordero, E. C., and P. M. de F. Forster (2006), Stratospheric variability and trends in models used for the IPCC AR4, *Atmos. Chem. Phys.*, *6*, 5369–5380, doi:10.5194/acp-6-5369-2006.

Dufresne, J.-L., and S. Bony (2008), An assessment of the primary sources of spread of global warming estimates from coupled atmosphere–ocean models, *J. Clim.*, *21*, 5135–5144.

Gerber, E. P., et al. (2012), Assessing and understanding the impact of stratospheric dynamics and variability on the Earth system, *Bull. Am. Meteorol. Soc.*, *93*, 845–859, doi:10.1175/BAMS-D-11-00145.1.

Hardiman, S. C., N. Butchart, and N. Calvo (2013), The morphology of the Brewer-Dobson circulation and its response to climate change in CMIP5 simulations, *Q. J. R. Meteorol. Soc.*, doi:10.1002/qj.2258.

Hawkins, E., and R. Sutton (2009), The potential to narrow uncertainty in regional climate predictions, *Bull. Am. Meteorol. Soc.*, *90*, 1095–1107.

Karpechko, A. Y. (2010), Uncertainties in future climate attributable to uncertainties in future Northern Annular Mode trend, *Geophys. Res. Lett.*, *37*, L20702, doi:10.1029/2010GL044717.

Karpechko, A. Y., and E. Manzini (2012), Stratospheric influence on tropospheric climate change in the Northern Hemisphere, *J. Geophys. Res.*, *117*, D05133, doi:10.1029/2011JD017036.

Knutti, R., D. Masson, and A. Gettelman (2013), Climate model genealogy: Generation CMIP5 and how we got there, *Geophys. Res. Lett.*, *40*, 1194–1199, doi:10.1002/grl.50256.

Kodera, K., K. Yamazaki, M. Chiba, and K. Shibata (1990), Downward propagation of upper stratospheric mean zonal wind perturbation to the troposphere, *Geophys. Res. Lett.*, *17*, 1263–l266, doi:10.1029/GL017i009p01263.

Kumar, A., J. Perlwitz, J. Eischeid, X. Quan, T. Xu, T. Zhang, M. Hoerling, B. Jha, and W. Wang (2010), Contribution of sea ice loss to Arctic amplification, *Geophys. Res. Lett.*, *37*, L21701, doi:10.1029/2010GL045022.

Kushner, P. J., and L. M. Polvani (2004), Stratosphere–troposphere coupling in a relatively simple AGCM: The role of eddies, *J. Clim.*, *17*, 629–639.

Limpasuvan, V., D. W. J. Thomspon, and D. L. Hartmann (2004), The life cycle of the Northern Hemisphere sudden stratospheric warmings, *J. Clim.*, *17*, 2584–2596.

Lorenz, D. J., and E. T. DeWeaver (2007), Tropopause height and zonal wind response to global warming in the IPCC scenario integrations, *J. Geophys. Res.*, *112*, D10119, doi:10.1029/2006JD008087.

McLandress, C., J. Perlwitz, and T. G. Shepherd (2012), Comment on "Tropospheric temperature response to stratospheric ozone recovery in the 21st century" by Hu et al. (2011), *Atmos. Chem. Phys.*, *12*, 2533–2540, doi:10.5194/acp-12-2533-2012.

Meehl, G. A., et al. (2007), Global climate projections, in *Climate Change 2007: The Physical Science Basis. Contribution of Working Group I to the Fourth Assessment Report of the Intergovernmental Panel on Climate Change*, edited by S. Solomon et al., pp. 747–845, Cambridge Univ. Press, Cambridge, U. K., and New York.

Omrani, N.-E., N. S. Keenlyside, J. Bader, and E. Manzini (2014), Stratosphere key for wintertime atmospheric response to warm Atlantic decadal conditions, *Clim. Dyn.*, *42*, 649–663, doi:10.1007/s00382-013-1860-3.

Pennell, C., and T. Reichler (2011), On the effective number of climate models, *J. Clim.*, *24*, 2358–2367.

Polvani, L. M., and D. W. Waugh (2004), Upward wave activity flux as a precursor to extreme stratospheric events and subsequent anomalous surface weather regimes, *J. Clim.*, *17*, 3548–3554.

Previdi, M., and L. Polvani (2012), Comment on "Tropospheric temperature response to stratospheric ozone recovery in the 21st century" by Hu et al. (2011), *Atmos. Chem. Phys.*, *12*, 4893–4896, doi:10.5194/acp-12-4893-2012.

Reichler, T., P. K. Kushner, and L. M. Polvani (2005), The coupled stratosphere–troposphere response to impulsive forcing from the troposphere, *J. Atmos. Sci.*, *62*, 3337–3352.

©2014. American Geophysical Union. All Rights Reserved.

Scaife, A. A., et al. (2012), Climate change projections and stratosphere–troposphere interaction, *Clim. Dyn.*, *38*, 2089–2097, doi:10.1007/s00382-011-1080-7.

Screen, J. A., and I. Simmonds (2010), The central role of diminishing sea ice in recent arctic temperature amplification, *Nature*, *464*, 1334–1337, doi:10.1038/nature09051.

Screen, J. A., I. Simmonds, C. Deser, and R. Tomas (2013), The atmospheric response to three decades of observed Arctic sea ice loss, *J. Clim.*, *26*, 1230–1248, doi:10.1175/JCLI-D-12-00063.1.

Shaw, T. A., M. Sigmond, and T. G. Shepherd (2009), Sensitivity of simulated climate to conservation of momentum in gravity wave drag parameterization, *J. Clim.*, *22*, 2726–2742.

Shindell, D. T., R. L. Miller, G. Schmidt, and L. Pandolfo (1999), Simulation of the Arctic oscillation trend by greenhouse forcing of a stratospheric model, *Nature*, *399*, 452–455, doi:10.1038/20905.

Sigmond, M., and J. F. Scinocca (2010), The influence of the basic state on the Northern Hemisphere circulation response to climate change, *J. Clim.*, *23*, 1434–1446, doi:10.1175/2009JCLI3167.1.

Son, S.-W., et al. (2010), Impact of stratospheric ozone on Southern Hemisphere circulation change: A multimodel assessment, *J. Geophys. Res.*, *115*, D00M07, doi:10.1029/2010JD014271.

Song, Y., and W. A. Robinson (2004), Dynamical mechanisms for stratospheric influences on the troposphere, *J. Atmos. Sci.*, *61*, 1711–1725.

SPARC CCMVal (2010), *SPARC Report on the Evaluation of Chemistry-Climate Models*, *SPARC Rep.*, *5*, edited by V. Eyring, T. G. Shepherd, and D. W. Waugh, pp. 149–190, SPARC, Toronto, Canada.

Stroeve, J. C., V. Kattsov, A. Barrett, M. Serreze, T. Pavlova, M. Holland, and W. N. Meier (2012), Trends in Arctic sea ice extent from CMIP5, CMIP3 and observations, *Geophys. Res. Lett.*, *39*, L16502, doi:10.1029/2012GL052676.

Taylor, K. E., R. J. Stouffer, and G. A. Meehl (2012), An overview of CMIP5 and the experiment design, *Bull. Am. Meteorol. Soc.*, *93*, 485–498, doi:10.1175/BAMS-D-11-00094.1.

Thompson, D. J. C., J. C. Furtado, and T. G. Shepherd (2006), On the tropospheric response to anomalous stratospheric wave drag and radiative heating, *J. Atmos. Sci.*, *63*, 2616–2629.

Thompson, D. W. J., and S. Solomon (2002), Interpretation of recent Southern Hemisphere climate change, *Science*, *296*, 895–899.

Thompson, D. W. J., and J. M. Wallace (2000), Annular modes in the extratropical circulation. Part I: Month-to-month variability, *J. Clim.*, *13*, 1000–1016.

Woollings, T. (2008), Vertical structure of anthropogenic zonal-mean atmospheric circulation change, *Geophys. Res. Lett.*, *35*, L19702, doi:10.1029/2008GL034883.

Woollings, T., J. M. Gregory, J. G. Pinto, M. Reyers, and D. J. Brayshaw (2012), Response of the North Atlantic storm track to climate change shaped by ocean–atmosphere coupling, *Nat. Geosci.*, *5*, 313–317, doi:10.1038/NGEO1438.

©2014. American Geophysical Union. All Rights Reserved.